N.Ya. Ivanichok[1], P.I. Kolkovskyi[2], A.M. Soltys[1], V.M. Boychuk[1], V.I. Mandzyuk[1], L.S. Yablon[1], B.I. Rachiy[1]

The effect of orthophosphoric acid on energy-intensive parameters of porous carbon electrode materials

[1]*Vasyl Stefanyk Precarpathian National University, Ivano-Frankivsk, Ukraine, volodymyr.mandzyuk@pnu.edu.ua*
[2]*V.I. Vernadskii Institute of General and Inorganic Chemistry of the NAS of Ukraine, Kyiv, Ukraine*

The effect of orthophosphoric acid concentration as an activating agent on the porous structure of carbon materials derived from apricot pits and energy-intensive parameters of electrochemical capacitors formed on their basis is studied. It is found that changing the ratio of the mass of the activating agent to the mass of the raw material in acid-activated porous carbon materials (PCMs), one can control the pore size distribution in the range of 0.5-20 nm and specific surface area in the range of 775-1830 m^2/g. The use of cyclic voltammetry, impedance spectroscopy and chronopotentiometry made it possible to set the capacitive nature of charge accumulation processes in acid-activated PCMs, as well as to determine the contribution of a certain size of pores to the specific capacitance of PCM/electrolyte system.

Keywords: porous carbon material, activating agent, specific surface area, pore size distribution, specific capacity, electrochemical capacitor.

Introduction

Porous carbon materials (PCMs), having a number of unique properties, are widely used for purification of drinking water from organic impurities [1, 2], separation and storage of gases [3, 4], manufacturing electrodes of electrochemical capacitors (ECs) [5-8] and lithium power sources [9, 10]. Nowadays, PCMs are made from raw materials (RMs) of natural and artificial origin. Preference is given to the former because they are cheap and environmentally friendly. In recent years, research has been conducted to obtain PCMs from agricultural waste, such as cherry and apricot pits [11], coconut shells [12], corn cobs [13], flax and hemp fibers [14] and others. Apricot fruit is an important RM in the food industry, its seeds are used in medicine and cosmetology. Wastes of this production are apricot pits, which can be used as raw material for high-porosity carbon that also solves the problem of disposal of food waste, which leads to environmental pollution.

The most common methods for obtaining PCMs are physical or chemical activation of carbonaceous RMs [15-17], as well as methods of template synthesis [18, 19].

Chemical activation usually occurs at temperatures (400-800°C) and is accompanied by the use of dehydrating agents (phosphoric acid, zinc chloride, potassium hydroxide). Chemical activation is considered as a reaction between a solid precursor and a chemical reagent. The mass of the final product and its structure depend on the concentration and ratio of the source components, temperature and activation time. A necessary condition for chemical activation is the removal of residual activating reagents and inorganic residue contained in the original carbonized material. When chemically activating plant raw materials with orthophosphoric acid, the latter acts as a dehydrating agent that inhibits the formation of resin, which increases the mass yield of porous carbon and reduces the temperature and activation time compared to physical activation methods [20]. Mixing orthophosphoric acid with crushed apricot pits leads to fragmentation of cellulose, hemicellulose and lignin. The acid separates the cellulose

fibers and causes partial depolymerization of hemicellulose and lignin, which leads to a decrease in the mechanical strength of the particle and its swelling. Orthophosphoric acid leads to the primary carbonization of RM at this stage [20]. When obtaining activated carbon by chemical activation of RM with orthophosphoric acid, the ratio between the amount of acid and the precursor is important for the development of the porous structure of the product obtained. Therefore, the aim of this work is to study the effect of orthophosphoric acid concentration on the structure of PCM and energy-intensive parameters of ECs formed on its basis.

I. Materials and methods

The RM for the production of porous carbon was apricot pits, dried and ground to a fraction of 0.25-1 mm. The resulting material was divided into portions weighing 8 g and mixed with 50 g of orthophosphoric acid. The acid concentration varied from 4 to 32 % in increments of 4 %.The ratio of the mass of the activating agent to the mass of the raw material $Y = m(H_3PO_4)/m(RM)$ was respectively 0.25:1; 0.5:1; 0.75:1; 1:1; 1.25:1; 1.5:1; 1.75:1 and 2:1. The resulting mixture was stirred thoroughly for 1-2 hours, then dried at 100°C for 24 hours until a constant mass was reached. Then the mixture was placed in a vertical cylindrical furnace and heated to 550°C at speed of 10°C/min in an argon atmosphere at a gas flow rate of 30 ml/min. When the set temperature was reached, isothermal exposure was performed for 60 minutes. After cooling the material to room temperature, it was washed with hot distilled water to neutral pH and dried at 80°C until a constant mass was reached. The materials obtained are marked according to the ratio of the mass of acid to the mass of raw materials (Table 1).

Thermal transformations of the initial material and materials modified with orthophosphoric acid were studied using a synchronous thermal analyzer STA 449 F3 Jupiter (NETZSCH) in the linear heating mode at a rate of 10°C/min in an argon atmosphere at a gas flow rate of 30 ml/min and temperature range of 20-600°C. The change in mass of the studied samples as a result of heating is represented by the thermogravimetric (TG) curve (measurement accuracy 1 mg), the rate of mass change is represented by the differential thermogravimetric (DTG) curve. An empty crucible of Al_2O_3 was used as a reference standard. The test sample was heated together with the reference sample and the current temperature of the test sample and the temperature difference between the sample and the standard were recorded, which allowed to record the processes associated with the absorption or release of energy.

The textural characteristics of samples were analyzed on the basis of low-temperature (77.4 K) nitrogen

for 24 h. The specific surface area (S_{BET}) was calculated according to the standard Brunauer-Emmett-Teller (BET) method. The specific surface area (S_{micro}) and volume (V_{micro}) of micropores was calculated by t-method, surface (S_{meso}) and volume (V_{meso}) of mesopores were calculated as the difference between the total surface area (volume) of pores and micropores. The total pore volume V was evaluated from the nitrogen adsorption at $p/p_0 \approx 0.99$, where p and p_0 denote the equilibrium and saturation pressure of nitrogen at 77.4 K, respectively. Calculation of pore size distribution was performed by NLDFT (nonlocal density functional theory) method in the slit-shape pore approximation.

Electrochemical studies of the PCM/electrolyte system were performed in three-electrode cells (Fig. 1). The working electrode (1) was formed of PCM, conductive additive and binder material in a ratio of 75:20:5 wt. %, respectively. A silver chloride (Ag-AgCl) electrode (2) was the reference electrode and the platinum electrode (3) was as the auxiliary one. The silver chloride electrode was placed in a 3.5 M aqueous KCl solution (6) and combined with the working chamber via an agar-agar salt bridge (5). A 30% aqueous solution of KOH was used as the electrolyte (4). The potential of the working electrode against the reference electrode was -0.33 – -0.28 V at room temperature.
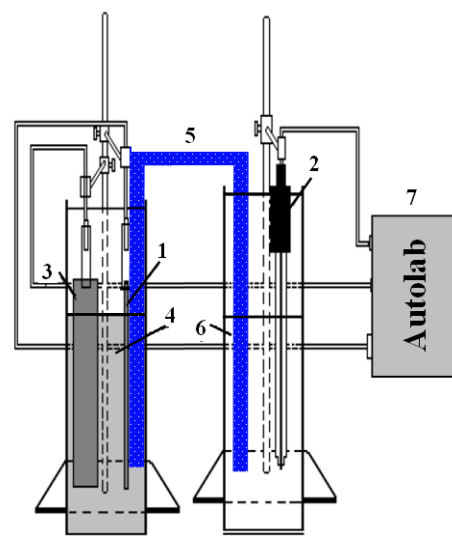
Fig. 1. Scheme of a three-electrode cell for electrochemical research.

The operational characteristics of laboratory samples of ECs were determined in a two-electrode cell (Fig. 2).

Button-type EC electrodes were prepared by pressing a mixture of PCM, conductive additive, and binder material in a ratio of 75:20:5 wt. % respectively into a nickel grid. The formed electrodes were separated by a separator and placed in a two-electrode cell, which was

Table 1.

Designation of acid-activated PCMs

Y	0.25	0.50	0.75	1.00	1.25	1.50	1.75	2.00
Sample	C025	C050	C075	C100	C125	C150	C175	C200

adsorption-desorption isotherms recorded using a Quantachrome Autosorb Nova 2200c adsorption analyzer. Before measurements, the samples were heated at 180°C

sealed after filling with electrolyte.
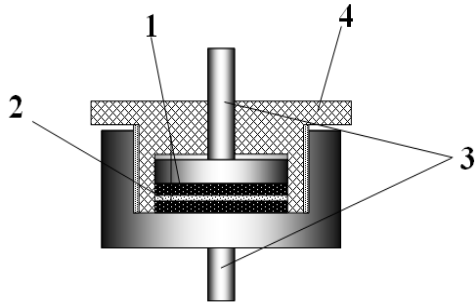
Fig. 2. The scheme of the cell for measuring the capacity of the EC: 1 – electrodes, 2 – separator, 3 – current taps, 4 – insulating cover.

Methods of cyclic voltammetry, impedance spectroscopy and chronopotentiometry were used to study the electrochemical properties of ECs with electrodes on the basis of PCMs. Measurements were performed using an Autolab spectrometer ("ECO CHEMIE", the Netherlands), equipped with GPES and FRA-2 software.

Cyclic voltammograms were obtained in the potential range from -1 to 0.2 V for three-electrode cells and from 0 to 1 V for two-electrode cells at a scan rate s $1 \div 50$ mV/s. Voltammetry determines the dependence of current on the applied potential, which changes periodically and linearly over time with a rate $s = \pm \frac{dU}{dt}$. The corresponding current of capacitor with capacitance C is determined as $I = C\frac{dU}{dt} = C \cdot s$. The EC capacity is determined as $C = I/s$ at low scan rate [21]. The total charge accumulated on the electrode surface is calculated by integrating the function $C(U, t)$ over time $q = \int_{u_2}^{u_1} C(U)\frac{dU}{dt} dt = \int_{u_2}^{u_1} C(U)dU$. Capacity is calculated as the ratio of total charge to the magnitude of the potential window $C = q/U$, in which the study is conducted. To estimate the effectiveness of the EC the dependence of the capacity on the scan rate is determined.

Impedance hodographs (or Nyquist diagrams) $Z'' = f(Z')$, where Z' and Z'' are real and imaginary parts of the complex resistance of the system, respectively, were obtained in the frequency range 10^{-2} - 10^5 Hz. The amplitude of the sinusoidal voltage was 10 mV.

Chronopotentiometric studies were performed in the voltage range $0 \div 1$ V, the charge/discharge current of the capacitor varied in the range from 10 to 50 mA in increments of 10 mA. The specific capacity of the electrode material of the EC was calculated by the formula

$$C = \frac{2It}{(U_{max} - \Delta U)m},$$

where I – charge/discharge current, t – discharge time, U_{max} – maximal voltage, ΔU – voltage drop when the discharge circuit is closed, m – mass of PCM.

II. Results and discussion

Fig. 3 presents TG and DTG curves obtained for plant raw materials due to heating to a temperature of 600°C. In the range of 50-200°C the decrease in the mass of the test samples by 8-10 % is due to the removal of sorbed water contained in the material. When the temperature reaches 250°C, the process of carbonization and decomposition of hemicellulose and cellulose begins, which lasts up to 450°C and is accompanied by 55% weight loss. The next temperature range (450-600°C) is associated with the formation of semi-coke with a small weight loss of 5 %.
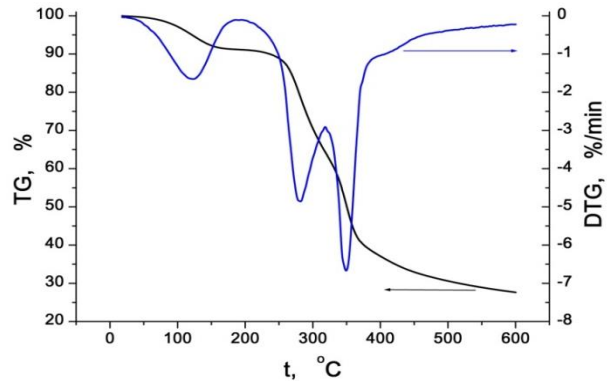

Fig. 3. Thermogram of raw material.

The results of thermogravimetric studies for materials impregnated with orthophosphoric acid at values of $Y = 0.25$ and 0.50 (samples C025, C050) are presented in Fig. 4.

The first region of weight loss due to sorbed forms of water is practically absent on these thermograms. Most probably, orthophosphoric acid at low concentrations first reacts with hemicellulose and lignin, which leads to a sharp drop in mass starting from 100°C (Fig. 4, a). The weight loss with increasing temperature slows down to 0.5 %/min after 450°C. The final oxidation of carbon material after reaction with acid takes place at this stage. The total weight loss of RM is 45% in this temperature range. The temperature of cellulose carbonization decreases at a higher content of orthophosphoric acid, which follows from the presence of only one peak on the DTG curve (Fig. 4, b). In the temperature range of 150-500°C, micro- and mesopores are formed, which is a consequence of the interaction of orthophosphoric acid with biopolymers (lignin, hemicellulose and cellulose). Further increase in the concentration of orthophosphoric acid does not lead to differences in TG and DTG curves for PCMs (Fig. 5). The total weight loss is 40-50 % for all samples, which is less compared to the initial RM.

Orthophosphoric acid acts as an activating agent and promotes dehydration of the primary material, which reduces the degradation temperature of the material, increases the mass of the obtained carbonized carbon material and promotes the formation of its porous structure.

According to low-temperature porometry (Table 2), PCMs are characterized by a microporous structure (the contribution of micropores is 95%) and a developed surface area at low concentrations of orthophosphoric acid (samples C025, C050, C075). Samples C100 and C125 have the maximum value of the specific surface area (1600-1850 m^2/g), which is mainly provided by micropores (90-95 %). The maximum total pore volume 1.231 cm^3/g, which is provided by mesopores (about 57 %), is typical for the sample C150. As Y increases

a)

b)
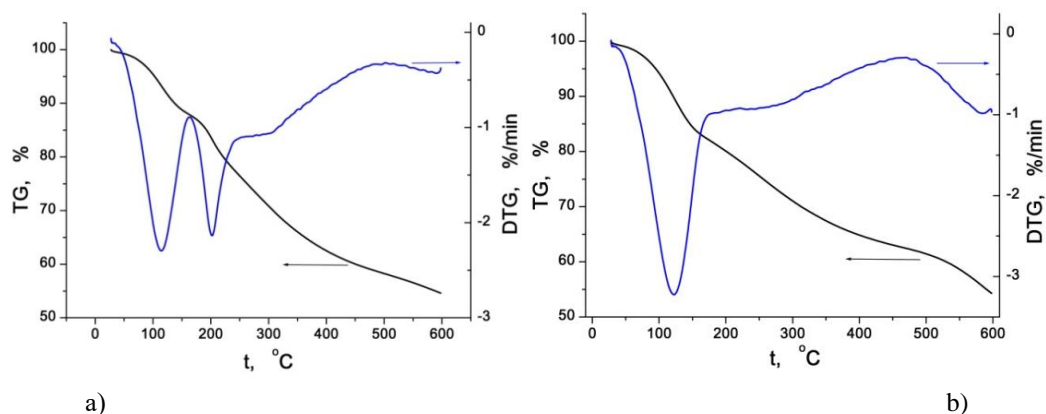
Fig. 4. Thermogram of samples C025 (a) and C050 (b).

a)

b)

c)

d)

e)

f)
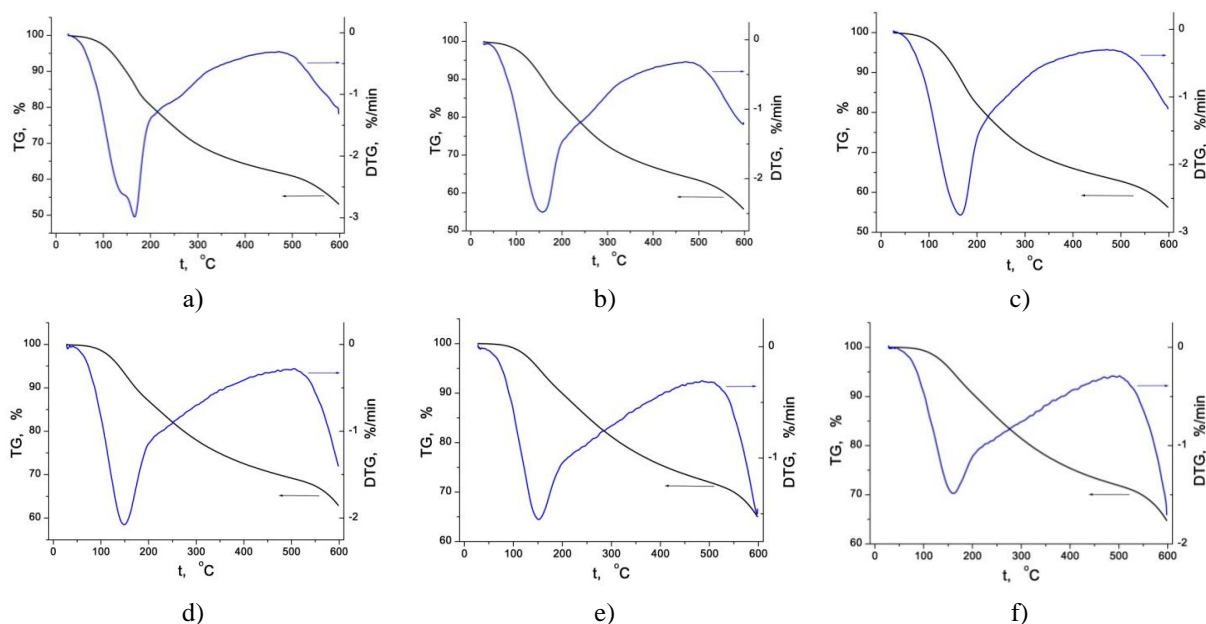
Fig. 5. Thermogram of samples C075 (a), C100 (b), C125 (c), C150 (d), C175 (e), and C200 (f).

further, both the total surface area and the pore volume of PCMs decrease (samples C175 and C200). Thus, changing the ratio of Y from 0.25 to 1.25, one can obtain microporous carbon material, and when $Y = 1.25 \div 2.00$ mesopores are formed, which are about 50% of the total area and 75% of the total volume.

Table 2.
Structural and adsorption characteristics of PCMs

| Sample	S_{BET}, m²/g	S_{micro}, m²/g	S_{meso}, m²/g	V, cm³/g	V_{micro}, cm³/g	V_{meso}, cm³/g
C025	775	745	30	0.336	0.303	0.033
C050	880	870	10	0.360	0.354	0.006
C075	1340	1290	50	0.575	0.535	0.040
C100	1635	1520	115	0.804	0.687	0.117
C125	1830	1760	70	0.856	0.779	0.077
C150	1510	645	865	1.231	0.319	0.912
C175	1335	712	623	1.095	0.334	0.761
C200	1120	560	560	0.851	0.243	0.608

According to cyclic voltammetry results (Fig. 6 and Fig. 7) it follows that for acid-activated PCMs there are no redox peaks in the studied potential range that indicates the electrostatic interaction of electrolyte ions with the developed electrode surface. There is a pronounced asymmetry with respect to zero current depending on the

scanning rate s, as well as a difference in the amount of charge during anodic and cathodic polarization at low values s (1-5 mV/s). The asymmetry of these curves with respect to the potential of zero charge indicates the difference between the value of the accumulated charge by K⁺ ions and OH⁻ groups. The magnitude of the current in the negative potential range exceeds the value of the corresponding currents in the positive region by 1.5-2 times, which indicates the dominance of charge accumulation due to K⁺ ions, according to the reaction:

$$C_x + K^+ + e^- \leftrightarrow C^-_x \parallel K^+,$$
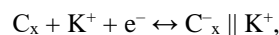
where C_x – the surface of the porous structure of the carbon material; K⁺ – electrolyte cations; $\parallel$ – double electric layer (DEL), where the charge accumulates due to mechanism of physical adsorption [21].

There is an increase in the specific surface area from 770 to 1800 m²/g (Fig. 6, b, d, f) when $0.25 \leq Y \leq 1.25$, but a correlation between currents on voltammograms (Fig. 6, a, c, e) and the specific surface area is not observed. The voltammograms of PCMs are almost indistinguishable at low scan rates and $0.25 \leq Y \leq 1.00$, although the surface doubles. Samples C100 and C125 have a larger specific

a)

b)

c)

d)

e)

f)
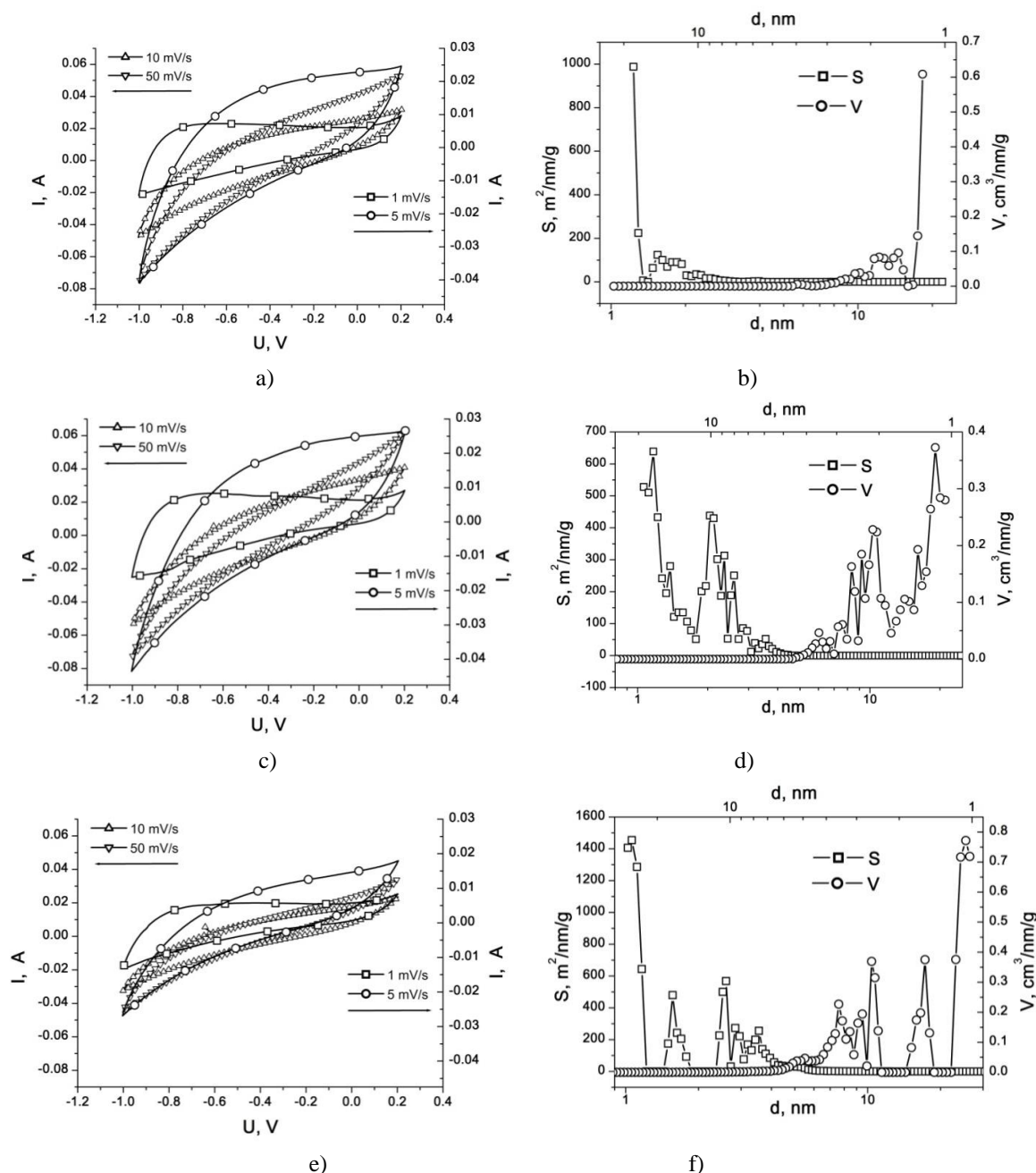
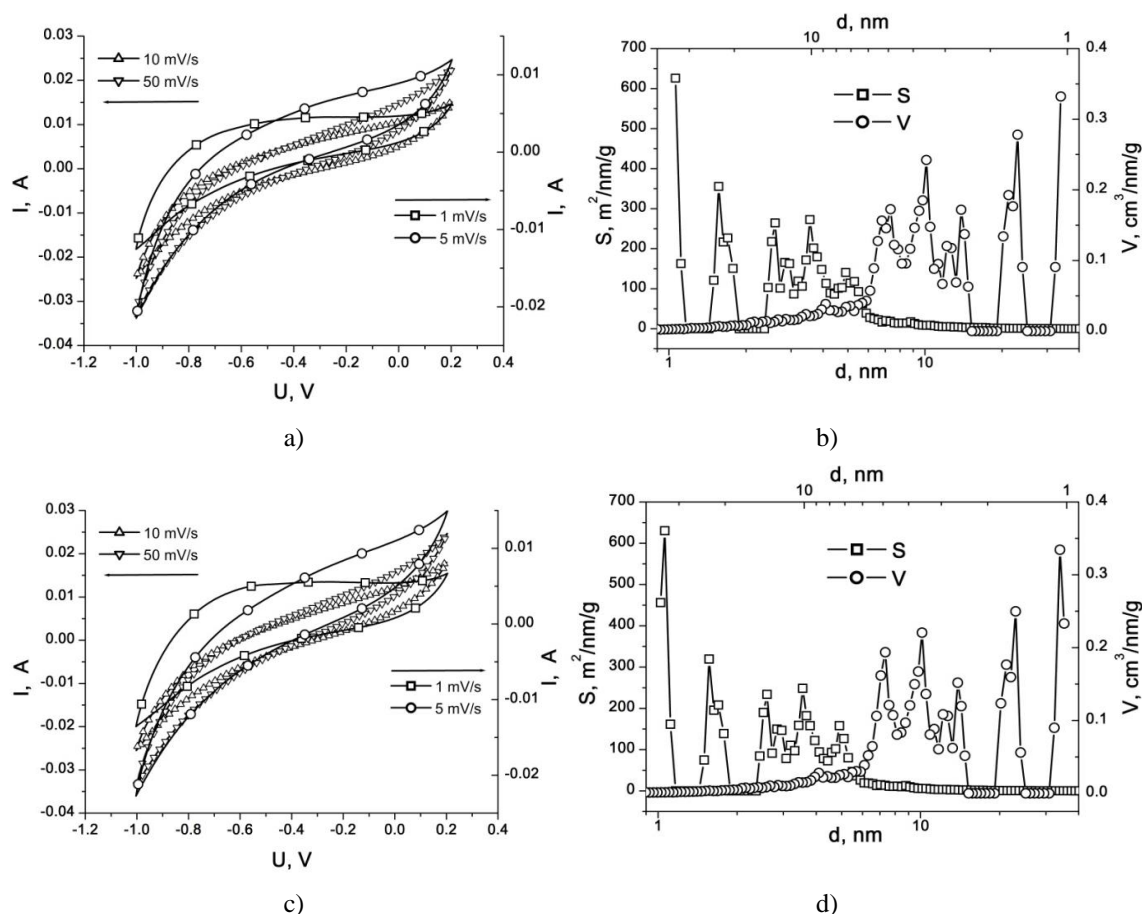**Fig. 6.** Cyclic voltammograms and pore size distribution for samples C025 (a, b), C075 (c, d), C125 (e, f).

surface area compared to other materials, but the cycling currents are slightly lower than for samples at $Y < 1$. One of the reasons is the large number of pores smaller than 1 nm (Fig. 6, f), which make significant contribution to the size of the surface area, but are difficult to access for electrolyte ions during cycling. Increasing the scan rate above 10 mV/s leads to distortion of voltammetry shapes, which is a consequence of increased internal resistance due to low electrical conductivity of these materials as they are obtained at 550°C.

Voltammograms for mesoporous carbon materials are close to rectangular ones in the positive potential range at low scanning rates (Fig. 7). In this region the charge accumulates due to the formation of DEL by hydroxyl groups on the carbon surface. Low mobility of OH^- groups leads to a change in the course of voltammograms when the scan rate increases slightly.

The values of the specific capacity of PCMs depending on the scan rate are given in Table 3.

According to Table 3, the maximum capacity of the PCM/KOH system is achieved when using PCM with a pore distribution in the range of 1-3 nm, i.e. for microporous materials with a small proportion of transport mesopores.

Laboratory models of EC were made on the basis of samples with the maximum specific capacity (C075, C100, and C125). The cyclic voltammograms of the ECs show that their shape and magnitude of anode and cathode currents are the same at low scan rates (1-5 mV/s) (Fig. 8). An increase in scan rate over 5 mV/s leads to a maximum on the voltammograms in the potential range of 0.2-0.6 V. This effect is especially evident for a series of carbon materials with a microporous structure and a large specific surface area (Fig. 8, c).

a)

b)

c)

d)

Fig. 7. Cyclic voltammograms and pore size distribution for samples for mesoporous carbon materials C175 (a, b) and C200 (c, d).

Table 3.

Specific capacity (F/g) of acid-activated PCMs at different scan rate and a potential -0.4 V

| Sample	1 mV/s	2 mV/s	3 mV/s	4 mV/s	5 mV/s	10 mV/s
C025	99.2	92.7	82.0	69.1	61.0	23.2
C050	132.8	119.8	101.7	84.1	72.8	25.7
C075	140.7	123.8	101.9	82.1	68.7	34.3
C100	148.4	130.4	108.0	85.3	69.7	40.0
C125	99.1	71.3	52.8	39.6	32.0	15.7
C150	61.4	25.9	16.6	11.5	8.8	4.0
C175	76.4	45.3	31.4	22.2	12.4	8.7
C200	68.6	45.8	26.3	18.5	9.3	7.0

The change in the shape of voltammograms is due to the rapid increase in the concentration of ions on the surface of the electrodes with a slight increase in the EC potential, which leads to an increase in the current [22]. The largest value of the current corresponds to a potential of 0.2 V (Fig. 8, c), around which the concentration of ions is maximum. Further accumulation of ions on the surface of the electrodes becomes more complicated and slows down, which is manifested in a decrease in the current value with increasing EC potential.

The internal resistance of the EC increases when $s \geq 20$ mV/s. As a result, the shape of the voltammogram changes during the transition from capacitive to resistive one and the specific capacity of PCM decreases several times (Fig. 9).

The properties of the electrochemical system PCM/electrolyte depending on the applied electrode potential were studied by impedance spectroscopy method. The obtained Nyquist diagrams (Fig. 10) make it possible to estimate the effect of the porous structure of carbon material and its electrical characteristics on the system parameters depending on the ions of the electrolyte used. The values of the specific capacity and electrical resistance of PCM at different values of the electrode potential provide important information about the effectiveness of its use as an electrode material of EC.

The Nyquist diagrams have the form characteristic of ECs with a dominant capacitive charge accumulation process at the PCM/electrolyte interface in the potential range -1 ÷ -0.4 V (Fig. 10). It is expressed by an almost vertical section on the diagram at low frequencies. When the electrode potential increases from -0.4 to 0.2 V, a semicircle appears on all hodographs in the high-frequency region, which is associated with the passing of

a)   b)

c)
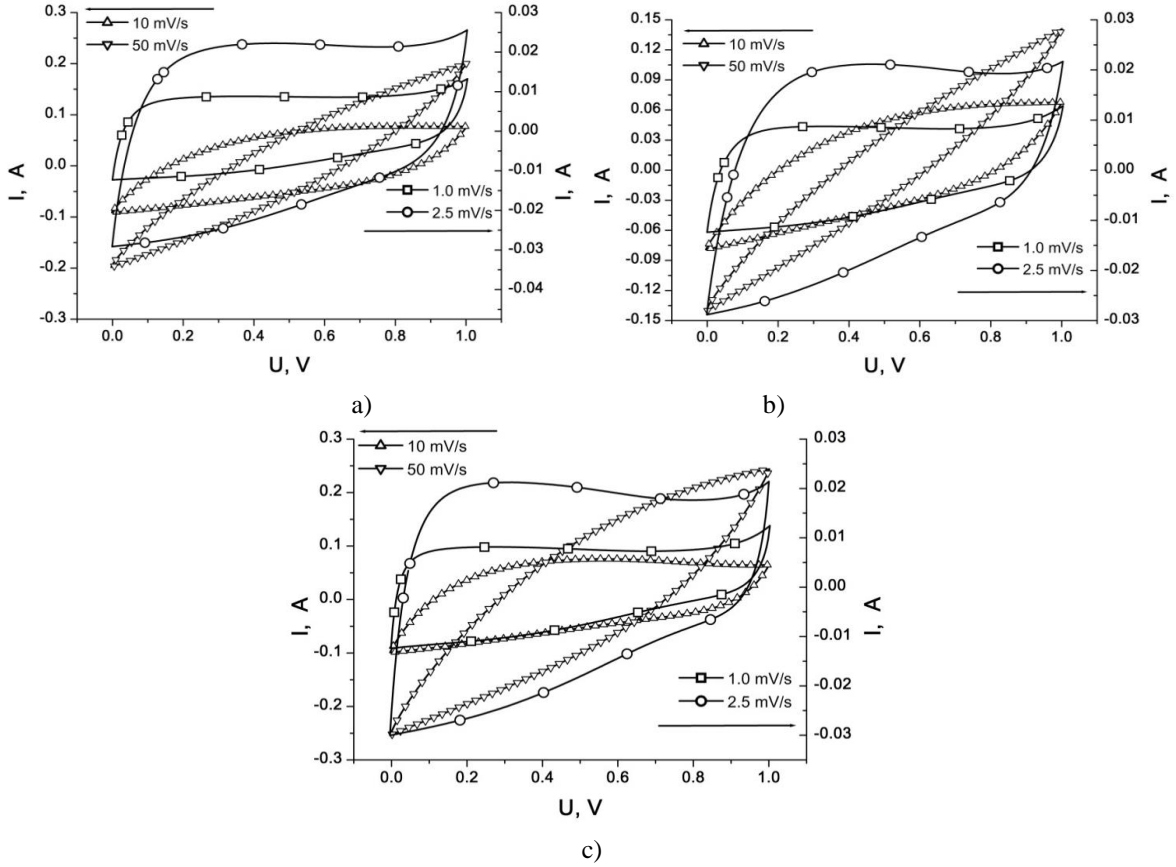
Fig. 8. Cyclic voltammograms for ECs based on samples C075 (a), C100 (b), and C125 (c).
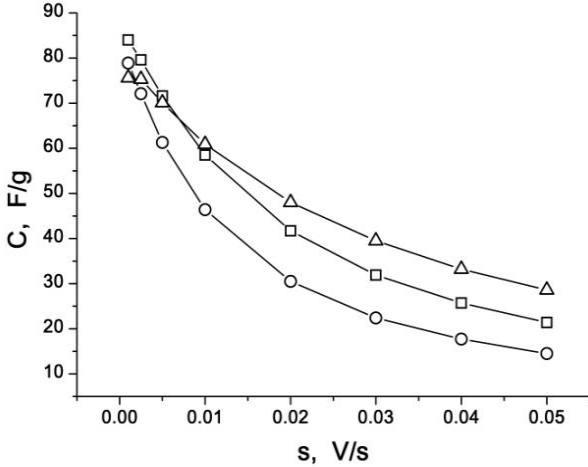
Fig. 9. Dependence of the specific capacity of PCMs on the scan rate for samples C075 (-○-), C100 (-□-), and C125 (-Δ-).

Faraday processes at the electrode [23]. In this case, redox

reactions occur with the participation of OH⁻ groups. Nyquist diagrams in the range of middle and low frequencies are represented by a straight line with different angles of inclination, which depends on the applied potential, and characterizes the different mechanisms of charge accumulation in the PCM/electrolyte system. The increase of the electrode potential in the positive region leads to a decrease in the angle of inclination of the hodograph within $40º \leq \varphi \leq 50º$, which indicates the diffusion processes in this electrochemical system.

To establish the relationship between the porous structure and the specific capacity of PCM in aqueous solution of KOH, Nyquist diagrams are modeled by an equivalent electrical circuit or determine the specific capacity using calculation formulas that do not require model assumptions [24]. The total complex resistance in an alternating current circuit according to Ohm's law is equal to:

$$Z^* = \frac{U_0 e^{j\omega\tau}}{I_0 e^{j(\omega\tau+\varphi)}} = \frac{U_0}{I_0} e^{-j\varphi} = Z\cos\varphi - jZ\sin\varphi = Z' - jZ'',\qquad(1)$$

where U_0, I_0 – voltage and current amplitudes, ω – angular frequency, φ – phase shift angle, j – imaginary unit ($j = \sqrt{-1}$).

a) b)

c) d)
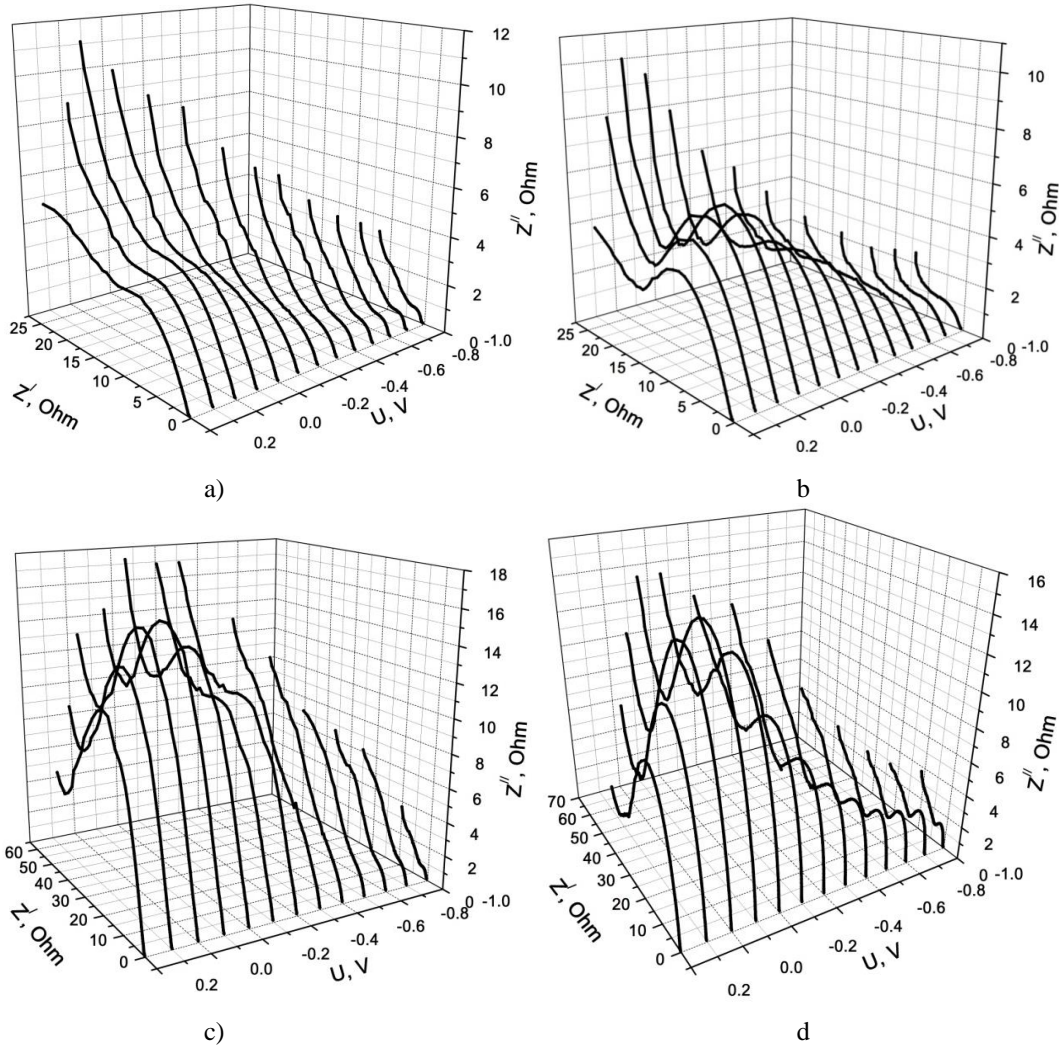
Fig. 10. Nyquist diagrams for PCM/KOH systems based on samples C025 (a), C075 (b), C125 (c), and C200 (d) at different applied potentials.

The electrical resistance R is the main element in impedance models. In the frequency region $Z_R(j\omega) = R$ simulates the proportional relationship between the parameters of the state (current and voltage) and reflects the lack of phase shift between these parameters. The impedance of this element reflects the frequency-independent component of the substance, i.e. Re $Z_R = R$, and Im $Z_R = 0$.

The parameter $1/C$ is the coefficient of proportionality between the voltage U_C and the integral from the function of the time dependence of current, which passesthrough this element and is characterized by the ratio $U_C(t) = \frac{1}{C}\int_{t_0}^{t} i(t)dt + U_C(t_0)$. This relationship is written as $(j\omega) = \frac{1}{j\omega C} = -\frac{j}{\omega C}$ in the frequency region. Element Z_C contains only the reactive component, which for positive C values is negative one, i.e. reflects the phase delay at $\pi/2$. The impedance Z_C decreases proportionally with increasing frequency. The voltage of the element is proportional to the charge accumulated by it.

Impedance hodographs of studied electrochemical systems (Fig. 10) indicate that there is a pseudo-capacitive accumulation of energy in addition to the DEL capacity. The obtained hodographs can be modeled by equivalent

schemes shown in Fig. 11.

Theoretically, these schemes are described as follows [25]:

$$\frac{1}{Z} = \frac{1}{1/j\omega C_{dl}} + \frac{1}{R_F + 1/j\omega C_p} = j\omega C_{dl} + \frac{j\omega C_p}{j\omega R_F C_p + 1}, \quad (2)$$

where C_{dl} – DEL capacity, C_p – pseudocapacity, R_F – Faraday resistance.

At very low frequencies ($\omega \to 0$), and/or low R_F

$$\frac{1}{Z} = j\omega(C_{dl} + C_p), C = C_{dl} + C_p.$$

At sufficiently high frequencies ($j\omega R_F C_p \gg 1$)

$$Z = \frac{R_F}{1 + j\omega R_F C_{dl}}.$$

The total capacity of the system is calculated using equation (2) at $\omega \to 0$ (Fig. 12).

The specific capacity of PCMs depends on the magnitude of the electrode potential (Fig. 12), due to changes in the free charge of the surface during its polarization in the positive or negative direction. Conducting electrochemical studies in a three-electrode
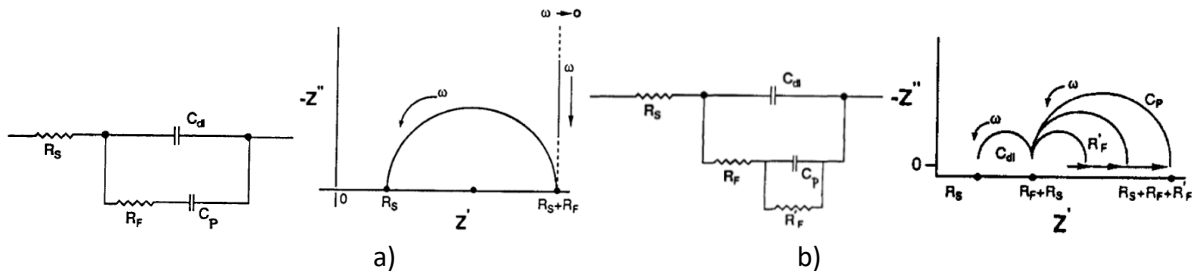
Fig. 11. The simplest equivalent schemes of ECs and their hodographs [25].
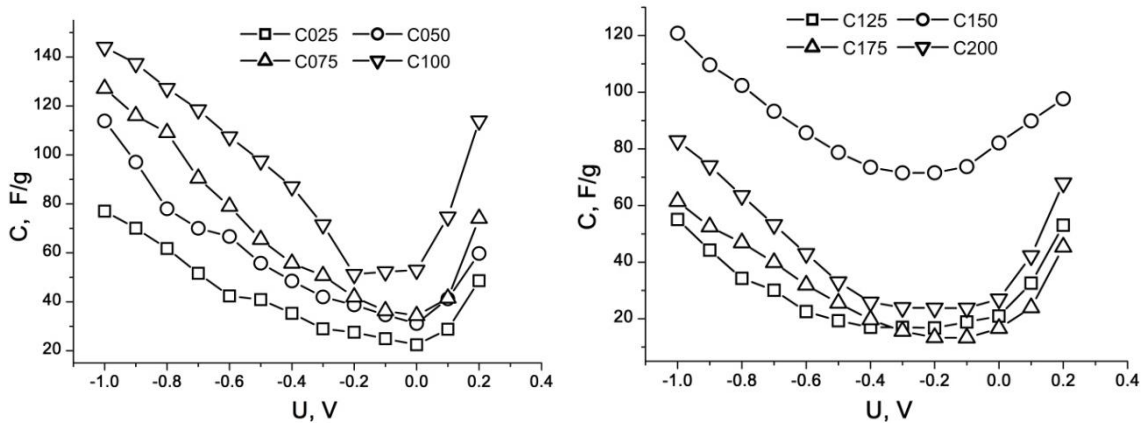

Fig. 12. Dependence of the specific capacity of PCMs on the electrode potential.

cell, it was found that the potential of carbon material against the reference electrode was -0.33 – -0.28 V. There is the minimum on volt-farad dependences in range of these potentials. This minimum corresponds to the potential of zero charge in the absence of specific effects on the electrode surface [26] and is shifted to the positive side, which is due to the adsorption of molecular oxygen on the PCM surface in the KOH electrolyte [27]. The specific capacity of PCMs is 15-45 F/g at the potential of zero charge that indicates the ability to spontaneous charge of the porous structure, which occurs according to electrostatic mechanism.

The maximum specific capacitance of PCMs is 150 F/g at negative polarization and decreases with increasing of electrode potential. The capacity is reduced by 25-40 % in the region of positive potentials (0.1-0.2 V). Stationary potentials of carbon materials are in the range of -0.25 – 0.05 V, in which DEL is formed by hydrated electrolyte ions [21]. This region is characterized by an increase in capacity at negative polarization and its decreasing at positive polarization. The use of an aqueous solution of KOH as an electrolyte leads to a change in the chemical potentials of ions. As a result the window of potentials of the DEL charge according to the electrostatic mechanism expands from -0.01 ÷ -0.25 V [21] to -0.01 ÷ -0.49 V [27]) and the shift of work potentials with the contribution of electrosorption of hydrogen (from -0.25 ÷ -0.65 V to -0.49 ÷ -0.9 V). Positive polarization in the range of -0.01 ÷ 0.1 V leads to electrosorption of hydroxyl groups [27]. At high positive potentials (above 0.2 V) the electrosorption process can lead to an increase in irreversible reactions, such as the formation of water molecules.
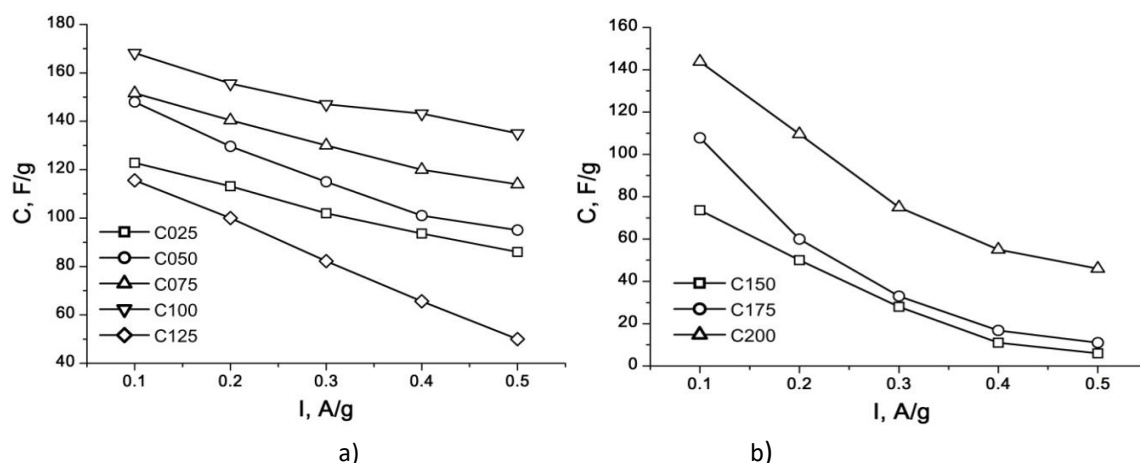
To set the correlation between the specific surface area of pores of different diameters and the capacity of the PCM/electrolyte system, the specific capacity of PCMs was determined by chronopotentiometric method at different operating currents (Fig. 13).

Given that the potassium ion may have two hydrate shells with radii of 0.266 and 0.36 nm [28], it is assumed that pores with a diameter greater than 0.5 nm are electrochemically available for charge in the KOH electrolyte [29]. Both the size of the electrolyte ion and the pore size will affect the maximum DEL. The highest energy of adsorption interaction of PCM with electrolyte molecules is observed in narrow pores of 0.5-1 nm in size. Pores larger than 2 nm are as transport channels for the electrolyte to enter the working pores.

The relationship between the specific surface area of PCM (Table 4) and the specific capacity value (Fig. 13) can be traced.

As follows from Table 4, an increase in the pore area of 1.25-1.65 nm in size leads to an increase in the specific capacity of PCM. For samples C075 and C100, in addition to a given range of pores, a significant contribution to the total area is made by pores of 2.05-2.65 nm in size, which serve as transport channels for the electrolyte. The contribution of transport pores is manifested in the minimal reduction of the specific capacitance with increasing discharge current. Carbon materials C125 ÷ C175, in which pores with a size of 1.05-1.25 nm predominate, have a specific capacity of 35-50 % lower than previous samples, which is probably due to the presence of pores only in a narrow range. The presence of pores of 1.25-1.45 nm in size with significant area (554 m^2/g) for sample C200 provides to the increase in the capacity of PCM. However, a small number of pores in the range of 1.65-1.85 nm leads to a sharp decline in its specific capacity with a slight increase in discharge current. Thus, by changing the ratio of the mass of the

The effect of orthophosphoric acid on energy-intensive parameters of porous carbon electrode materials

a)   b)

Fig. 13. Dependence of specific capacitance on discharge current for microporous (a) and mesoporous (b) carbon materials.

Dependence of the specific surface area (m^2/g) of PCMs on the pore size

Pore size, nm	Sample							
	C025	C050	C075	C100	C125	C150	C175	C200
1.05-1.25	0	0	0	0	1048	486	414	0
1.25-1.45	620	751	885	790	118	6	15	554
1.45-1.65	9	20	40	54	3	57	1	2
1.65-1.85	2	12	24	26	60	65	43	48
1.85-2.05	7	14	22	13	17	27	21	23
2.05-2.25	27	23	62	67	0	1	0	0
2.25-2.45	26	20	64	107	0	35	0	0
2.45-2.65	15	7	37	75	23	47	9	10
2.65-2.85	12	9	36	68	81	53	36	41
2.85-3.05	6	2	15	40	37	36	26	29
3.05-3.25	4	2	9	32	31	31	23	25

activating agent (orthophosphoric acid) to the mass of plant raw materials, one can effect the pore size distribution of PCM, which in turn allows you to control its specific electrical capacity.

Conclusions

According to thermogravimetric studies, the addition of 4-8% orthophosphoric acid to the raw material leads to a sharper drop in mass with increasing temperature compared to the initial material, due to the simultaneous interaction of acid with sorbed water, hemicellulose and lignin. Orthophosphoric acid causes the dehydration of the initial material, which leads to a decrease in the temperature of material degradation, increase the mass of the PCM obtained and promotes the formation of its porous structure.

Carbon material with a microporous structure and a total pore volume 0.86 cm^3/g is formed at a growth of Y from 0.25 to 1.25. A further increase Y from 1.25 to 2 results in the formation of mesopores 5-50 nm in size, which is 75 % of the total pore volume.

It was found that the accumulation of capacity in the ECs is due to the formation of DEL at the electrode/electrolyte interface and pseudocapacity. The maximum capacity of the PCM/KOH system is achieved by using microporous carbon materials C075-C125 with a small proportion of transport mesopores, which have a pore distribution in the range of 1-3 nm.

Ivanichok N.Y. – Candidate in Physics and Mathematics, Doctoral Student, Leading Specialist of Joint Educational and Scientific Laboratory for Physics of Magnetic Films;
Kolkovskyi P.I. – Candidate in Physics and Mathematics, Senior Researcher;
Soltys A.M. – PhD Student;
Boychuk V.M. – Doctor in Physics and Mathematics, Professor of Department of Physics and Methods of Teaching;
Mandzyuk V.I. – Doctor in Physics and Mathematics, Professor of Department of Computer Engineering and Electronics;
Yablon L.S. – Doctor in Physics and Mathematics, Professor of Department of Physics and Methods of Teaching;
Rachiy B.I. – Doctor in Physics and Mathematics, Professor of Department of Materials Science and New Technologies.

N.Ya. Ivanichok, P.I. Kolkovskyi, A.M. Soltys, V.M. Boychuk, V.I. Mandzyuk, L.S. Yablon, B.I. Rachiy

[1] V.D. Canh, S. Tabata, S. Yamanoi, Y. Onaka, T. Yokoi, H. Furumai, H. Katayama, *Evaluation of Porous Carbon Adsorbents Made from Rice Husks for Virus Removal in Water,* Water, 13(9), Art. 1280 (2021); https://doi.org/10.3390/w13091280.

[2] J. Li, R. Holze, S. Moyo, S. Wang, S. Li, T. Tang, X. Chen, *Three-dimensional hierarchical porous carbon derived from natural resources for highly efficient treatment of polluted water,* Environ. Sci. Eur., 33, Art. 98 (2021); https://doi.org/10.1186/s12302-021-00527-6.

[3] S. Sircar, T.C. Golden, M.B. Rao, *Activated Carbon for Gas Separation and Storage*, Carbon, 34(1) 1 (1996); https://doi.org/10.1016/0008-6223(95)00128-X.

[4] Y. Wu, B.M. Weckhuysen, *Separation and Purification of Hydrocarbons with Porous Materials*, Angew, Chem. Int. Ed., 60(35), 18930 (2021); https://doi.org/ 10.1002/anie.202104318.

[5] B.I. Rachiy, I.M. Budzulyak, E.A. Ivanenko, S.L. Revo, *A composite of nanoporous carbon and thermally exfoliated graphite as an effective electrode material for supercapacitors*, Surface Engineering and Applied Electrochemistry, 51(5), 501 (2015); https://doi.org/10.3103/S1068375515050129.

[6] Y.Y. Starchuk, B.I. Rachiy, I.M. Budzulyak, P.I. Kolkovskyi, N.Y. Ivanichok, M.O. Halushchak, *Electrochemical Properties of Hybrid Supercapacitors Formed Based on Nanoporous Carbon and Nickel Tungstate,* Journal of Nano- and Electronic Physics, 13(6), Art. 06021 (2021); https://doi.org/10.21272/jnep.13(6).06021.

[7] V. Boichuk, V. Kotsyubynsky, A. Kachmar, B. Rachiy, L. Yablon, *Effect of Synthesis Conditions on Pseudocapacitance Properties of Nitrogen-Doped Porous Carbon Materials*, Journal of Nano Research, 59, 112(2019); https://doi.org/10.4028/www.scientific.net/JNanoR.59.112

[8] V.I. Mandzyuk, I.F. Myronyuk, V.M Sachko, B.I. Rachiy, Yu.O. Kulyk, I.M. Mykytyn, *Structure and Electrochemical Properties of Saccharide-derived Porous Carbon Materials*, Journal of Nano- and Electronic Physics, 10(2), Art. 02018 (2018); https://doi.org/ 10.21272/jnep.10(2).02018.

[9] V.I. Mandzyuk, N.I. Nagirna, R.P. Lisovskyy, *Morphology and Electrochemical Properties of Thermal Modified Nanoporous Carbon as Electrode of Lithium Power Sources,* Journal of Nano- and Electronic Physics, 6(1) Art. 01017 (2014).

[10] R. Wang, R. Wu, C. Ding, Z. Chen, H. Xu, Y. Liu, J. Zhang, Y. Ha, B. Fei, H. Pan, *Porous Carbon Architecture Assembled by Cross-Linked Carbon Leaves with Implanted Atomic Cobalt for High-Performance Li–S Batteries,* Nano-Micro Letters, 13(1), Art. 151 (2021); https://doi.org/10.1007/s40820-021-00676-6.

[11] B.I. Rachiy, B.K. Ostafiychuk, I.M. Budzulyak, N.Y. Ivanichok, *Specific Energy Characteristics of Nanoporous Carbon Activated by Orthophosphoric Acid,* Journal of Nano- and Electronic Physics,7(4), Art. 04077 (2015).

[12] K.-C. Lee, M.S.W. Lim, Z.-Y. Hong, S. Chong, T.J. T., G.-T. Pan, C.-M. Huang, *Coconut Shell-Derived Activated Carbon for High-Performance Solid-State Supercapacitors,* Energies, 14, Art. 4546 (2021); https://doi.org/10.3390/en14154546.

[13] S. Yang, K. Zhang, *Converting Corncob to Activated Porous Carbon for Supercapacitor Application,* Nanomaterials, 8(4), Art. 181 (2018); https://doi.org/10.3390/nano8040181.

[14] R.Ya. Shvets, I.I. Grygorchak, A.K. Borysyuk, S.G. Shvachko, A.I. Kondyr, V.I. Baluk, A.S. Kurepa, B.I. Rachiy, *New nanoporous biocarbons with iron and silicon impurities: synthesis, properties, and application to supercapacitors*, Phys. Solid State, 56(10), 2021 (2014); https://doi.org/10.1134/s1063783414100266.

[15] J. Zhou, A. Luo, Y. Zhao, *Preparation and characterisation of activated carbon from waste tea by physical activation using steam,* Journal of the Air & Waste Management Association, 68(12), 1269 (2018); https://doi.org/10.1080/10962247.2018.1460282.

[16] N.Ya. Ivanichok, O.M. Ivanichok, B.I. Rachiy, P.I. Kolkovskyi, I.M. Budzulyak, V.O. Kotsyubynsky, V.M. Boychuk, L.Z. Khrushch, *Effect of the carbonization temperature of plant biomass on the structure, surface condition and electrical conductive properties of carbon nanoporous material*, Journal of Physical Studies 25(3), Art. 3801 (2021); https://doi.org/10.30970/jps.25.3801.

[17] I.F. Myronyuk, V.I. Mandzyuk, V.M Sachko, R.P. Lisovskyy, B.I. Rachiy, *Morphological and Electrochemical Properties of the Lactose-derived Carbon Electrode Materials,* Journal of Nano- and Electronic Physics 8(4), Art. 04006 (2016); https://doi.org/10.21272/jnep.8(4(1)).04006.

[18] C. Wang, B. Yan., J. Zheng, L. Feng, Z. Chen, Q. Zhang, T. Liao, J. Chen, S. Jiang, C. Du, S. He, *Recent progress in template-assisted synthesis of porous carbons for supercapacitors,* Advanced Powder Materials 1(2), Art. 100018 (2022); https://doi.org/10.1016/j.apmate.2021.11.005.

[19] V.I. Mandzyuk, I.F. Myronyuk, V.M Sachko, I.M. Mykytyn, *Template Synthesis of Mesoporous Carbon Materials for Electrochemical Capacitors*, Surf. Eng. Appl. Electrochem. 56(1), 93 (2020); https://doi.org/10.3103/S1068375520010123.

[20] W.C. Lim, C. Srinivasakannan, N. Balasubramanian, *Activation of palm shells by phosphoric acid impregnation for high yielding activated carbon*, J. Anal. Appl. Pyrolysis, 88(2), 181 (2010); https://doi.org/10.1016/j.jaap.2010.04.004.

[21] A.I. Belyakov, A.M. Brintsev, N. Khodyrevskaya, Proc. 14-th International Seminar on Double Layer Capacitors and Hybrid Energy Storage Devices. Deerfield Beach, USA. 84 (2004).

[22] H. Wang, L. Pilon,*Physical interpretation of cyclic voltammetry for measuring electric double layer capacitances*, Electrochim. Acta 64, 130 (2012); (https://doi.org/10.1016/j.electacta.2011.12.118).

[23] K.D. Pershina, K.O. Kazdobin, Impedance spectroscopy of electrolytic materials (Osvita Ukrainy, Kyiv, 2012).

[24] E. Barsoukov, J.R. Macdonald, Impedance spectroscopy: theory, experiment, and applications (John Wiley & Sons Inc., New Jersey, 2018).

[25] B.E. Conway, Electrochemical supercapacitors: scientific fundamentals and technological applications (Kluwer-Plenum, New York, 1999).

[26] E. Lust, Encyclopedia of Interfacial Chemistry. Surface Science and Electrochemistry. Elsevier Inc. 316 (2018); https://doi.org/10.1016/B978-0-12-409547-2.13613-3.

[27] B.P. Bahmatyuk, A.S. Kurepa, I.I. Grygorchak, *Impedance spectroscopy of supercapacitors based on nanoporous activated carbon material*, Journal of National University "Lvivska Politechnika" "Physical & mathematical sciences" 687, 188 (2010).

[28] M.N. Rodnikova, S.A. Zasypkin, G.G. Malenkov, *About the mechanism of negative hydration,* Reports of the Academy of Sciences, 324(2), 368 (1992).

[29] E. Frackowiak, F. Beguin, *Carbon Materials for the Electrochemical Storage of Energy in Capacitors,* Carbon 39(6), 937 (2001); https://doi.org/10.1016/S0008-6223(00)00183-4.

Н.Я. Іванічок[1], П.І. Колковський[2], А.М. Солтис[1], В.М. Бойчук[1], В.І. Мандзюк[1], Л.С. Яблонь[1], Б.І. Рачій[1]

Вплив ортофосфорної кислоти на енергоємні параметри пористих вуглецевих електродних матеріалів

[1]Прикарпатський національний університет імені Василя Стефаника, Івано-Франківськ, Україна, *volodymyr.mandzyuk@pnu.edu.ua*
[2]Інститут загальної та неорганічної хімії імені В.І. Вернадського НАН України, Київ, Україна

У роботі досліджено вплив концентрації ортофосфорної кислоти як активуючого агента на пористу структуру вуглецевих матеріалів, отриманих із кісточок абрикоса, та енергоємні параметри електрохімічних конденсаторів, сформованих на їх основі. Встановлено, що в кислотноактивованих пористих вуглецевих матеріалах (ПВМ), змінюючи відношення маси активуючого агенту до маси вихідної сировини, можна контролювати розподіл пор за розмірами в межах 0,5-20 нм та питому площу поверхні в діапазоні 775-1830 м^2/г. Використання методів циклічної вольтамперометрії, імпедансної спектроскопії та хронопотенціометрії дало можливість встановити ємнісний характер процесів накопичення заряду в кислотноактивованих ПВМ, а також визначити вклад пор певного розміру в питому електроємність системи ПВМ/електроліт.

Ключові слова: пористий вуглецевий матеріал, активуючий агент, питома поверхня, розподіл пор за розмірами, питома ємність, електрохімічний конденсатор.